2020 IEEE/RSJ International Conference on Intelligent Robots and Systems (IROS)
October 25-29, 2020, Las Vegas, NV, USA (Virtual)

Semi-Autonomous Control of Leader-Follower Excavator using Admittance Control for Synchronization and Autonomy with Bifurcation and Stagnation for Human Interface

Kohei Iwano[1] and Masafumi Okada[1]

Abstract— **So far, multiple LCD monitors and joysticks have been used for remote operation of excavators while it has low work efficiency. This is because it is difficult for the operator to recognize the state of the excavator and its surrounding environment. We have developed a semi-autonomous control system which consists of autonomy (attractor based dynamical system) and human action (admittance control). On the other hand, excavation tasks require the task selection. In this paper, we propose a nonlinear dynamical system with attractor with stagnation and bifurcation.The stagnation of the attractor is designed as a negative divergence vector field that converges to a point on the trajectory. A stagnation is placed at a bifurcation point of the trajectory, and the operator selects the next task by adding a force to the leader system.**

I. Introduction

At disaster/mining sites, remote operation of hydraulic excavators has been carried out to ensure the safety of workers, and it also improves the working environment that involves long-distance travel to remote mining sites [1]. In conventional methods, multiple LCD monitors (displaying side-view, front-view, and first-person view) and control joy sticks have been installed [2]. However, it has been reported that those method decrease the work efficiency to less than 50% comparing to on-site operation [2]. This is because it is difficult for the operator to recognize the state of the hydraulic excavator and the surrounding environment with limited information.

So far, some studies have been conducted on improving operator's environmental awareness. For visual information, computer graphics of the robot and task objects are presented to the operator using a monitor [3]. A virtual bird's-eye view images are generated from the images of the multiple fish-eye cameras attached to the robot [4]. Moteki et al. discussed necessary visual information and necessity of haptic information [5]. Hirabayashi et al. proposed a remote control system with a haptic function for underwater construction machines [6]. On the other hand, to provide a realistics presence at a real field, a 3-DOF motion base is used for cock-pit to present vibration and tilt of the excavator [7]. Auditory feedback compensated the insufficient leader-follower force feedback information [8]. However, there are still considerable limitations on the amount of information that can be transmitted and delays due to electrical communication.

[1]The authors are with the Department of Mechanical Engineering, Tokyo Institute of Technology, Meguro-ku 152-8552, Japan okada.m.aa@m.titech.ac.jp

To overcome these limitations, it is effective to make excavators autonomomous. The autonomy of excavators is expected to support human operation (in a human-robot collaboration) and reduce the amount of information and telecommunication. The purpose of this paper is to design a semi-autonomous control and human interface for leader-follower system for excavators. It consists (a) the leader-follower system using admittance control and (b) attractor based autonomous control.

(a) Leader-follower system [9] plays roles of force sense presentation and intuitive human interface. So far, various types of leader-follower systems have been proposed and evaluated based on some evaluation criteria (e.g., stability and transparency) [10][11]. As the leader-follower system in this study, we use symmetric bilateral control [10] combined with admittance control. In admittance control [12][13], a robot is controlled to a position calculated based on a preset dynamic characteristic, using a measured value of a force sensor as input. Admittance control is used to magnify the operational force in physical human-robot interaction (pHRI) where the effects of inertia and joint friction are significant.
In our semi-autonomous system, for precise autonomous operation, the leader-follower robots are high-gain position controlled to prevent the external forces from the environment or operator. Thus, the human operation needs to be measured by a force sensor. The measured operational force is converted to the reference velocity, and it is added to the reference velocity of autonomy. An external force which acts on the follower system (excavator) also has to be transfers to the operator, however, a force sensor cannot be mounted on the follower system because of tough and dusty environment. To overcome these problems, admittance control and symmetric bilateral control (both are position-based) is introduced.

(b) Autonomous control for semi-autonomous control require flexibility of motions for human action. Because semi-autonomy includes human action, the control algorithm must be designed online while the precise operation also requires high-gain feedback and the predefined trajectories. So far, we have proposed a vector field-based controller (attractor-based controller [14]). This controller is represented by a nonlinear dynamical

system with attractor that converge to the specified trajectory. Because a reference is calculated based on the current state of the robot using vector field, the proposed method easily accepts the interposition of the operator. Moreover, because a reference trajectory is embedded into the vector field as an attractor, a stable motion is generated. Therefore, we use an attractor-based autonomous control system.

On the other hand, disadvantages of the conventional attractor-based controller are that (1) only one trajectory is embedded into the vector field, and (2) it is difficult to change the embedded trajectory on-line because it requires re-calculation of the vector field. They are fatal problems for excavation because it includes task selection (e.g., selection of digging in front or back) as shown in Fig.1. To overcome these problems, in this paper, we introduce stagnation and bifurcation of attractor. As shown in Fig.1, the stagnation is located on the bifurcation point of the trajectory, which is represented by a negative divergence of vector field. By the operator adding a force through the leader system, the robot gets out from the stagnation, and it continues its work. The operator selects the next work by the direction of the force. The proposed methods are illustrated in this paper and experimental evaluations are conducted using a prototype of the leader-follower system. Owing to the proposed semi-autonomous system, the leader system has a role of not only control rod but also informative device allowing real world miniature.

Recently, researches have been conducted on semi-autonomous systems that can switch between different tasks in pHRI using dynamical systems. Pistillo et al. proposed a method to encode several tasks in one dynamical system, and the operator can select a task by moving the robot [15]. This method has achieved task selection, but the trajectories of tasks are not connected directly and require more human effort. Okada and Nakamura designed a continuous symbol space which includes the vector field in the motion space that generates the cyclic motion and the continuous motion transition of the robots [16]. Khoramshahi and Billard switched multiple dynamical systems embedding different tasks based on human interaction [17]. These methods allows the robot for transitions between encoded tasks while they have been verified on single robot such as a humanoid robot and a collaborative robot, but not on a leader-follower robot. Both leader and follower robots have to maintain the equilibrium in their motion transition. Switching the dynamical system could break the equilibrium of the leader-follower robot and generate unexpected motion. We contribute to these literatures by proposing semi-autonomous leader-follower system with the task selection in a single dynamical system with a continuous bifurcated trajectory.

Section II introduces the configuration of the semi-autonomous system, Section III introduces the design of the human action (the admittance control), and Section IV introduces the design of the autonomous controller. In Section V, we perform verification experiments on the proposed method and report the results. Finally, in Section VI we conclude our work.

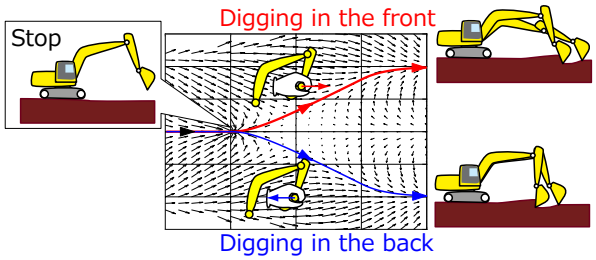

Fig. 1. Vector field with bifurcation and stagnation

II. Control System for Semi-Autonomous

Fig.2 shows a block diagram of the leader-follower semi-autonomous control system. Velocity based PI controllers (i.e., position based PD controllers) are used for each joint of the leader and follower, and the reference velocities are generated by the autonomous controller and the admittance controller. The subscripts l and f represent the leader and follower robot, respectively. Each robot is a three-link manipulator working in a vertical plane. $\boldsymbol{x} = \begin{bmatrix} x & y & \phi \end{bmatrix}^T$ is the position of a robot, where x and y are the position of the bucket's root, and ϕ is the absolute angle of the bucket. $\dot{\boldsymbol{x}}^{auto} \in \mathbb{R}^3$ denotes the reference velocity generated by the autonomous controller, and $\dot{\boldsymbol{x}}^{ad} \in \mathbb{R}^3$ is the reference velocity generated by admittance controller G.

The leader-follower semi-autonomous system includes autonomous control system and admittance controller (i.e., human action). Without human action, the leader-follower robots move following the autonomous control system. Thus, the autonomous control system reduces the amount of human operation. Human action on the autonomous control system is calculated using the admittance control. Owing to the admittance control, the operator can also percept the environmental information which is external force and position error between leader and follower. This system enables human action on the autonomous control system when the additional task or emergency operation is required.

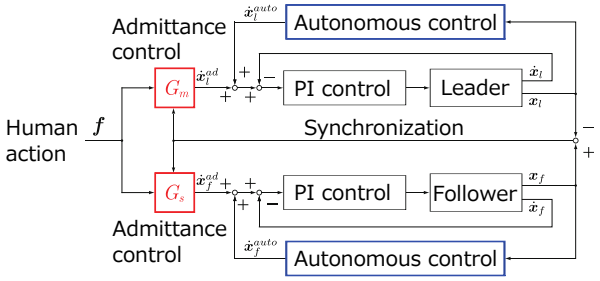

Fig. 2. Block diagram of the leader-follower semi-autonomous control system

III. Design of Human Action

A. Admittance controller

The role of the admittance controller is to magnify the operational force on the leader robot and to synchronize the

leader-follower robots. For the admittance control, we set the virtual dynamics (i.e. admittance) so that the leader and follower robots is electrically connected. Based on the admittance output, the reference velocities of the next step of the leader-follower robots are calculated using the operational force measured by the force/torque sensor mounted on the handle of the leader robot.

B. Dynamics of admittance control

The admittance controllers are set as virtual equations of dynamics;

$$C_v^l(\dot{\boldsymbol{x}}_l^{ad} - \dot{\boldsymbol{x}}_f) + K_v^l(\boldsymbol{x}_l - \boldsymbol{x}_f) = \boldsymbol{f}_h \quad (1)$$

$$C_v^f(\dot{\boldsymbol{x}}_f^{ad} - \dot{\boldsymbol{x}}_l) + K_v^f(\boldsymbol{x}_f - \boldsymbol{x}_l) = \boldsymbol{f}_h \quad (2)$$

where $\boldsymbol{f}_h \in \mathbb{R}^3$ is the operational force/torque measured by the force/torque sensor mounted on the leader robot, and $C_v \in \mathbb{R}^{3\times3}$ and $K_v \in \mathbb{R}^{3\times3}$ are the virtual damping and stiffness, respectively. For high operability (i.e., fast response), the virtual mass is set to zero. (1) and (2) mean that the leader-follower robots behave as if they are connected by springs and dampers. Because of the virtual spring K_v, the leader and follower synchronize each other. Because of equation (1), the leader system takes haptic performance. (1) and (2) are discretized, and the reference velocities from the admittance controller are calculated as;

$$\begin{aligned}\dot{\boldsymbol{x}}_{l,k+1}^{ad} =& \dot{\boldsymbol{x}}_{f,k} + (C_{v,k}^l)^{-1}\boldsymbol{f}_{h,k} \\ & - (C_{v,k}^l)^{-1}K_{v,k}^l(\boldsymbol{x}_{l,k} - \boldsymbol{x}_{f,k})\end{aligned} \quad (3)$$

$$\begin{aligned}\dot{\boldsymbol{x}}_{f,k+1}^{ad} =& \dot{\boldsymbol{x}}_{l,k} + (C_{v,k}^f)^{-1}\boldsymbol{f}_{h,k} \\ & + (C_{v,k}^f)^{-1}K_{v,k}^f(\boldsymbol{x}_{l,k} - \boldsymbol{x}_{f,k})\end{aligned} \quad (4)$$

where k is the time step.

IV. Design of Autonomous Controller

A. Configuration of attractor-based autonomy

Fig.3 shows the configuration of the vector field of the autonomous control system, which allows the operator select the trajectory. It consists of the attractor to the excavation trajectory (with bifurcation) and the stagnation. The reference velocity $\dot{\boldsymbol{x}}_*^{auto}$ consists the attractor term $\boldsymbol{v}_*^{at} \in \mathbb{R}^3$ and the stagnation term $\boldsymbol{v}_*^{stg} \in \mathbb{R}^3$:

$$\dot{\boldsymbol{x}}_*^{auto} = \boldsymbol{v}_*^{at} + \boldsymbol{v}_*^{stg}. \quad (5)$$

The stagnation is defined as a negative divergence vector field that converges to a specified point as shown in Fig.3(b). The stagnation plays a role of a brief stop point on the attractor. When a human operational force toward either bifurcated trajectory is applied to the robot, the leader and follower get out from the stagnation and move along the selected trajectory. That's how bifurcated attractor and stagnation enable the operator to select a trajectory.

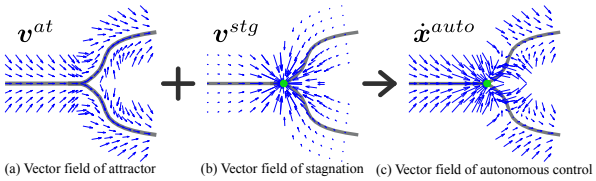

(a) Vector field of attractor (b) Vector field of stagnation (c) Vector field of autonomous control

Fig. 3. Configuration of the vector field of the autonomous control system

B. Design of dynamical system with attractor

We design a bifurcated attractor that enables the operator to select the work content. In this subsection, it is presented how to design dynamical system with attractor used in the proposed semi-autonomous system. The dynamical system with attractor is designed in three steps: 1) trajectory design, 2) vector field design, and 3) polynomial approximation.

1) Design of excavation trajectory with bifurcation: A specified trajectory Ξ is set as shown in Fig.4(a) in $\boldsymbol{x}$-space.

2) Design of vector field: As shown in Fig.4(b), points are set to be distributed near Ξ. On those points $\boldsymbol{X}_j \in \mathbb{R}^3$, velocity vectors $\boldsymbol{u}_j \in \mathbb{R}^3$ that converges to the trajectory are set. In this way, many sets of $(\boldsymbol{X}_j, \boldsymbol{u}_j)$ are obtained.

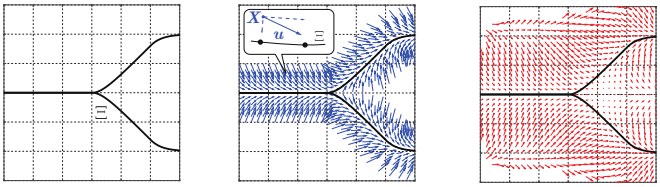

(a) Set of trajectory Ξ (b) Set of vector flow (c) Functional approximation

Fig. 4. Design of attractor

3) Controller design by polynomial: Based on the obtained $(\boldsymbol{X}_j, \boldsymbol{u}_j)$, the controller is designed by ℓ-th order polynomial approximation, using the same way as [14]. A calculated vector field is shown in Fig.4(c). The controller is represented by;

$$\boldsymbol{u} = \boldsymbol{a}_0 + \boldsymbol{a}_1\boldsymbol{X} + \boldsymbol{a}_2\boldsymbol{X}^2 + \cdots + \boldsymbol{a}_\ell\boldsymbol{X}^\ell \quad (6)$$

where $\boldsymbol{X}^i$ consists of $x^p y^q \phi^r$, and p, q and r are non-negative integers with $p+q+r=i$. Because (6) is written by;

$$\boldsymbol{u} = \boldsymbol{\Theta}\boldsymbol{\phi}(\boldsymbol{X}), \quad \boldsymbol{\Theta} = [\ \boldsymbol{a}_0 \quad \boldsymbol{a}_1 \quad \ldots \quad \boldsymbol{a}_\ell\ ] \quad (7)$$

$$\boldsymbol{\phi}(\boldsymbol{X}) = [\ 1 \quad \boldsymbol{X} \quad \boldsymbol{X}^2 \quad \ldots \quad \boldsymbol{X}^\ell\ ]^T \quad (8)$$

the coefficient matrix $\boldsymbol{\Theta}$ is given by p sets of $(\boldsymbol{X}_j, \boldsymbol{u}_j)$ as;

$$\boldsymbol{\Theta} = \boldsymbol{U}\boldsymbol{\Phi}^{\#} \quad (9)$$

$$\boldsymbol{U} = [\ \boldsymbol{u}_0 \quad \boldsymbol{u}_1 \quad \ldots \quad \boldsymbol{u}_p\ ] \quad (10)$$

$$\boldsymbol{\Phi} = [\ \boldsymbol{\phi}(\boldsymbol{X}_1) \quad \boldsymbol{\phi}(\boldsymbol{X}_2) \quad \ldots \quad \boldsymbol{\phi}(\boldsymbol{X}_p)\ ] \quad (11)$$

where $\boldsymbol{\Phi}^{\#}$ is defined by $\boldsymbol{\Phi}^T(\boldsymbol{\Phi}\boldsymbol{\Phi}^T)^{-1}$. In this paper, $\ell = 6$ is selected.

C. Design of stagnation

Because the stagnation is defined as a negative divergence vector field that converges to a specified point $\boldsymbol{x}_0 \in \mathbb{R}^3$, it is defined by;

$$\boldsymbol{v}_*^{stg} = -\frac{(\|W(\boldsymbol{x}_* - \boldsymbol{x}_0)\|^n)}{(\|W(\boldsymbol{x}_* - \boldsymbol{x}_0)\|^m + b)} A \frac{W(\boldsymbol{x}_* - \boldsymbol{x}_0)}{\|W(\boldsymbol{x}_* - \boldsymbol{x}_0)\|} \quad (12)$$

where m and n are the positive integers with $m > n$, which are set $m = 5$, $n = 2$ by preliminary experiments, and $W \in \mathbb{R}^{3\times3}$ is the weight matrix for scaling between components. Fig.5 shows the relationship between $\|W(\boldsymbol{x}_* - \boldsymbol{x}_0)\|$ (weighted relative distance of the robot with respect to stagnation point $\boldsymbol{x}_0$) and $\boldsymbol{v}^{stg}$. When $\|W(\boldsymbol{x}_* - \boldsymbol{x}_0)\|$ is zero, the velocity is zero, which yields a suspension of the motion. According to the inclease of $\|W(\boldsymbol{x}_* - \boldsymbol{x}_0)\|$, the velocity changes large that stands for suction to $\boldsymbol{x}_0$, and changes to zero with infinite value of $\|W(\boldsymbol{x}_* - \boldsymbol{x}_0)\|$, which means the stagnation does not work in the distance. The value of $A \in \mathbb{R}^{3\times3}$ changes the intension of suction, and the value of $b \in \mathbb{R}$ changes the value of r_0 that defines the area of the suction.

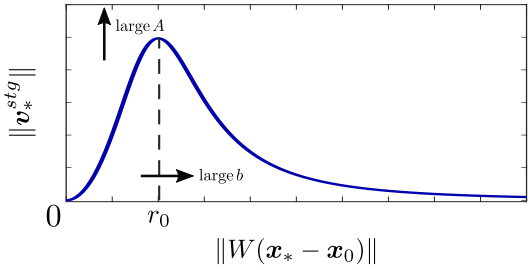

Fig. 5. Design of stagnation

V. Experimental Verification

A. Experimental setup

As shown in Fig.6, the 4-DOF leader-follower robots are prototyped which have homothetic shape of general hydraulic excavator. 90W DC motor and 150/1 reduction gear is utilized for Joint 2 while 60W DC motor and 100/1 reduction gear is utilized for Joint 1, 3, and 4. We use three joints except Joint 1. The leader and follower robot are the same size, and a force/torque sensor is mounted on the handle of the leader robot. Fig.7(a) shows the overall view of the experimental setup. During experiment, the operator looked at the side view of the follower robot displayed on the front display. Fig.7(b) shows the soil used in the experiments. Sand with 4∼7 mm size is used.

B. Verification of synchronization

To verify the synchronization of the leader and follower, the experiment is conducted using the admittance controller. In this experiment, the operator manually operated the robot to excavate. Fig.8 shows the motion of the leader and follower. The black solid line represents the motion of the leader in xy plane, the red dashed line represents the motion of the follower, and the orange solid line represents the height of the solid. The buckets on the trajectory represent

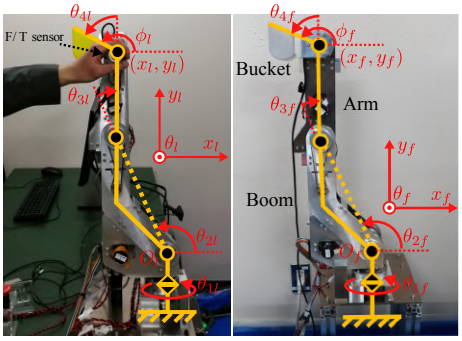

(a) Leader Robot (b) Follower Robot

Fig. 6. Leader-Follower excavation robot

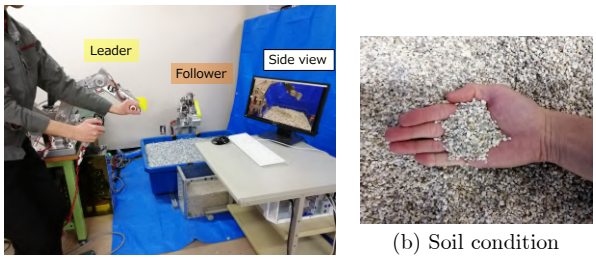

(a) Overall view (b) Soil condition

Fig. 7. Experimental setup

the orientations of the bucket at that time. The trajectory between the second and third buckets, highlighted by the blue arrows, is the trajectory where digging is actually taking place. The black solid line and the red dashed line almost overlap, which means that the motions of the leader and the follower are almost the same by the synchronization.

Fig.9(a) shows the absolute value of the position error between the leader and follower in xy components, and Fig.9(b) shows the absolute value of the operational force in xy components. Here, the part painted in blue represents the time of actual digging. While digging, the position error between leader and follower increases due to external environmental forces, and the operational force (the presentation force to the operator) changes according to the change of the position error, which means that haptic information in contact with an obstacle is transmitted to the operator.

C. Verification of stagnation and bifurcation

We implemented the autonomous control system including the stagnation and the bifurcated attractor. Fig.10 shows the designed trajectory with bifurcation. In this trajectory, the robots go down from the start point. Since the trajectory has bifurcation at point A into front and back, the operator will select an excavation trajectory. Finally, trajectories merge at the common end point. The stagnations were set at the places indicated by the green dots. A stagnation is also located at the start point, which allows the operator to decide the start of the work. At the second stagnation on point A, the operator selects the work.

Fig.11 shows the motion of the leader and follower in the experiment. The black solid line represents the motion of

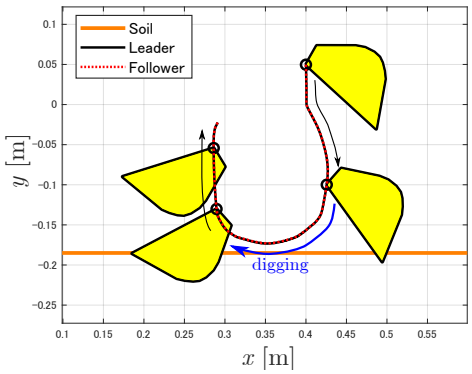

Fig. 8. Motion of the leader-follower in the digging with admittance control

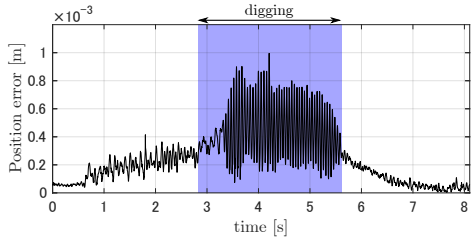

(a)Absolute value of the position error between the leader and follower

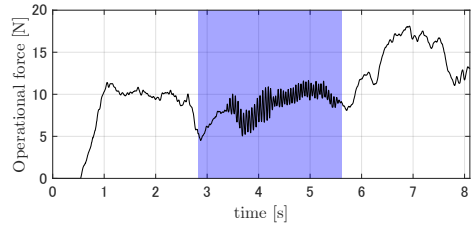

(b)Absolute value of the operational force in xy components

Fig. 9. Operational force and position error between the leader and follower in the digging with admittance control

the leader in xy plane, the red dashed line represents the motion of the follower, and the orange solid line represents the height of the soil. The buckets on the trajectory represent the orientations of the bucket at that time. Even in a semi-autonomous system, the leader and the follower performed the embedded operations with synchronization. The motion of the robots changes depending on whether it goes to back or front at the bifurcation point.

Fig.12(a) shows the time-lapse of the leader and follower robot and the trajectory of the root of the bucket. Fig.12(a)-(1-l) represents the initial position, and the first stagnation is set on this point. By added a force to downward direction by the operator, it starts to move and re-stops at the second stagnation shown in (2-l). The operator added a force to the back direction at this point, and the robot proceeds excavation along to the back trajectory shown in (3-l)∼(6-l) and (3-f)∼(6-f). On the other hand, in Fig.12(b)-(2-l), the operator added the forward force and the robot took the front trajectory. See the attached video for detailed robot motions. These results show that;

(i) by setting the stagnation, the robot stops and waits for an operator command.

(ii) the operator can select the next work by adding a force to leader system.

This operation is instinctive and easy to understand for the operator, which is realized by the proposed method.

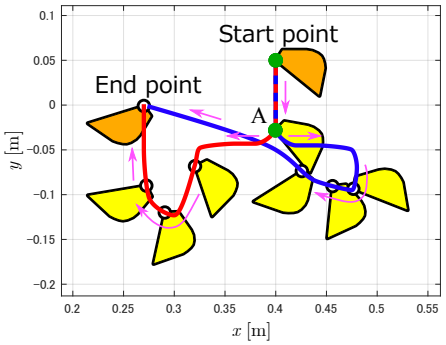

Fig. 10. Designed digging trajectory with bifurcation

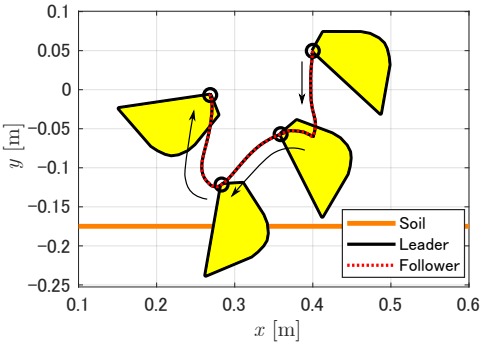

(a)Digging in the back

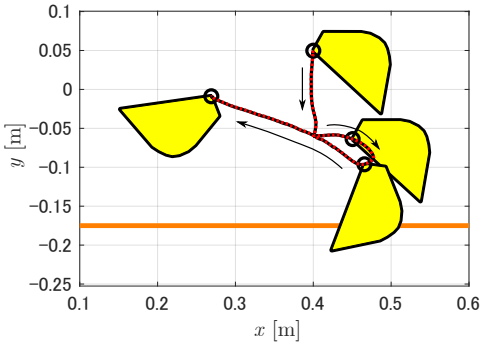

(b)Digging in the front

Fig. 11. Motion of the leader-follower by the semi-autonomous control with stagnation and bifurcation

VI. Conclusions

In this paper, for improvement of the efficiency of remote control of excavation, we proposed a semi-autonomous control system including the human action (admittance controller) and the autonomous control (attractor-based controller). The results are summarized as follows.

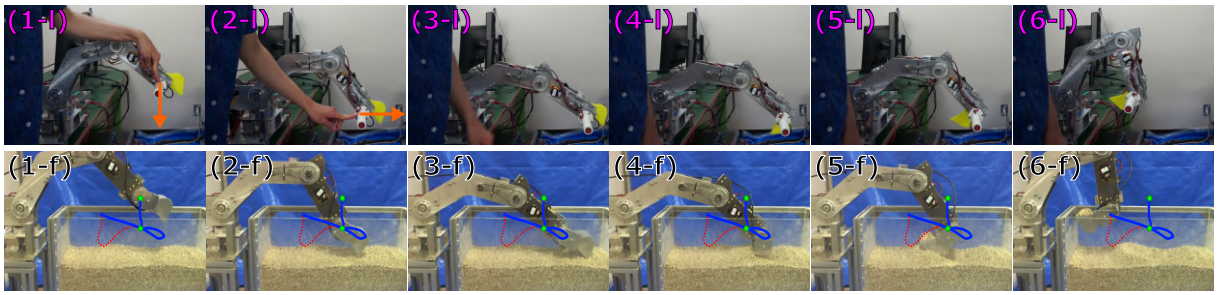

(a) Digging in the back

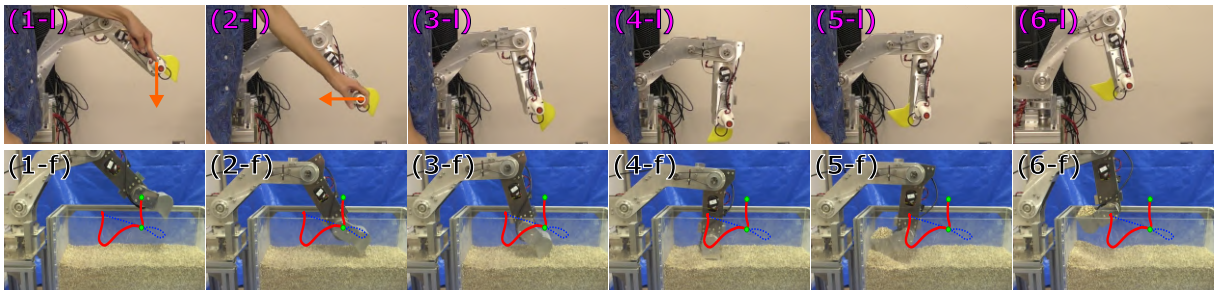

(b) Digging in the front

Fig. 12. Time-lapse of the leader-follower by the semi-autonomous control with stagnation and bifurcation

- In the proposed system, when there is not human action, the leader-follower robots basically move following the autonomous control system. By admittance control, the leader and follower perform almost the same motion with synchronizing.
- We introduced a semi-autonomous control system based on the stagnation and the bifurcation of attractor to realize the selection of work content.
  - Stagnation of attractor was designed as a negative divergence vector field that converged to a specified point on the trajectory, and the pause and resume of work was realized.
  - By designing an attractor for the excavation trajectory that has a bifurcation point and combining it with a stagnation, a selection of the attractor trajectory and selection of the work content have been realized by the operational force of the operator.

REFERENCES

[1] S. Ito, et al., "REMOTE CONTROLLED CONSTRUCTION EQUIPMENT BY USING HIGH-RESOLUTION STEREOSCOPIC 3D IMAGES (in Japanese)," Journal of Japan Society of Civil Engineers, Ser. F3 (Civil Engineering Informatics), 2017, vol.73, no.1, pp.15-24.

[2] G. Yamauchi, T. Hashimoto, and S. Yuta, "Assessment of Work Efficiency of HMD Viewing System for Unmanned Construction Work," ISARC. Proceedings of the International Symposium on Automation and Robotics in Construction, 2019, vol.36, pp. 824-830.

[3] H. Yamada, N. Tao, and Z. DingXuan, "Construction Tele-robot System With Virtual Reality," Proc. of 2008 IEEE Conference on Robotics, 2008, Automation and Mechatronics, pp. 36-40.

[4] T. Sato, et al, "Spatio-temporal bird's-eye view images using multiple fish-eye cameras," Proc. of 2013 IEEE/SICE International Symposium on System Integration, 2013, pp.753-758.

[5] M. Moteki, et al., "Research on improving work efficiency of unmanned construction," Proc. of 33rd International Symposium on Automation and Robotics in Construction, 2016, pp. 478-486.

[6] T. Hirabayashi, et al., "Teleoperation of construction machines with haptic information for underwater applications," Automation in construction, 2006, pp.563-570.

[7] H. Yamada, T. Kawamura, and K. Ootsubo, "Development of a teleoperation system for a construction robot," Journal of Robotics and Mechatronics, 2014, vol.26, no.1, pp.110-111.

[8] A. A. Yusof, T. Kawamura, and H. Yamada, "Operational Evaluation of a Construction Robot Tele-operation with Force Feedback," Transaction of The Japan Fluid Power System Society (JFPS), 2011, vol.43, no.1, pp.753-758.

[9] T. B. Sheridan, "Telerobotics," Automatica,1989, vol.25, no.4, pp.487-507.

[10] Y. Yokokohji and T. Yoshikawa, "Bilateral control of master-slave manipulators for ideal kinesthetic coupling-formulation and experiment," in IEEE Transactions on Robotics and Automation, vol. 10, no. 5, pp. 605-620

[11] D. A. Lawrence, "Stability and transparency in bilateral teleoperation," in IEEE Transactions on Robotics and Automation,1989, vol.25, no.4, pp.487-507.

[12] K. Furuta, K. Kosuge, Y. Shiote and H. Hatano, "Master-slave manipulator based on virtual internal model following control concept," Proceedings. 1987 IEEE International Conference on Robotics and Automation, Raleigh, NC, USA, 1987, pp. 567-572.

[13] A. Lecours, B. Mayer-St-Onge and C. Gosselin, "Variable admittance control of a four-degree-of-freedom intelligent assist device," 2012 IEEE International Conference on Robotics and Automation, Saint Paul, MN, 2012, pp. 3903-3908.

[14] M. Okada, K. Tatani, and Y. Nakamura, "Polynomial design of the nonlinear dynamics for the brain-like information processing of whole body motion," Proc. of 2002 IEEE International Conference on Robotics and Automation, 2002, pp.1410-1415.

[15] Pistillo, A., Calinon, S., and Caldwell, D. G. (2011). Bilateral physical interaction with a robot manipulator through a weighted combination of flow fields. In IEEE/RSJ international conference on intelligent robots and systems (IROS) (pp. 3047 寰?052).

[16] M. Okada and Y. Nakamura, "Design of the continuous symbol space for the intelligent robots using the dynamics-based information processing," IEEE International Conference on Robotics and Automation, 2004. Proceedings. ICRA '04. 2004, New Orleans, LA, USA, 2004, pp. 3201-3206 Vol.4.

[17] M. Khoramshahi and A. Billard, "A dynamical system approach to task-adaptation in physical human-robot interaction," Autonomous Robots, 2019, vol.43, no.4, pp.927-946.